

PARAMETERS CONTROLLING THE GENERATION AND PROPERTIES OF PLASMA SPRAYED ZIRCONIA COATINGS

P. Fauchais, M. Vardelle, A. Vardelle, L. Bianchi*, A.C. Léger

*L.M.C.T.S. - Equipe Plasma, Laser, Matériaux
Université de Limoges - URA CNRS 320 - Faculté des Sciences
123, Avenue Albert Thomas - 87060 LIMOGES Cedex - FRANCE*

** C.E.A.-D.A.M. BIII - B.P. 12
91680 BRUYERES-LE-CHÂTEL - FRANCE*

D.C. plasma jets temperature and velocity distributions as well as the arc root fluctuations at the anode were studied for Ar-H₂ (25 vol%) plasma forming gases. The parameters were the arc current up to 700 A, the total gas flow rate up to 100 slm, and the nozzle diameter which was varied from 6 to 10 mm. The trajectories of partially stabilized zirconia particles into the jet were studied by a 2D laser imaging technique and two fast (100 ns) two color pyrometers. The results have revealed the difficulty to inject small particles into the plasma flow since most were found to by-pass the jet rather than penetrate it. The results also show the broad trajectory distribution within the jet and the influence of the arc root fluctuations on the mean particle trajectory distribution within the jet. Beside the measurements of the particle surface temperature and velocity distributions in flight, the particle flattening and the cooling of the resulting splats were studied statistically for single particles all over the spray cone. Such studies have emphasized the drastic influence of the substrates or previously deposited layers temperature on the contact between them and the splats. At 200-300°C this contact is excellent (cooling rates of the order of 100 K/μs for 1 μm thick splats) and it results in a columnar growth within the splats and the layered splats of a bead (up to 500 layered splats). This growth can be observed through passes provided the bead surface

temperature has not cooled too much (a few tens of K) before the next bead covers it. A/C values up to 60 MPa were achieved with PSZ coatings. The effect of impact velocity of the particles, of substrate preheating temperature, of relative movements torch to substrate, of substrate oxidation on A/C values and splat formation were also studied.

NOTATIONS

a	: thermal diffusivity (m^2/s)
c_p	: specific heat at constant pressure ($\text{J}/\text{kg}\cdot\text{K}$)
D	: splat diameter (μm)
d	: nozzle internal diameter (mm)
d_i	: internal injector diameter (mm)
d_p	: particle diameter (μm)
E	: Young's modulus (GPa)
f	: restrike mode frequency (Hz)
I	: arc current (A)
L	: latent heat of fusion (J/kg)
m_{cg}	: carrier gas flow rate (slm)
m_g	: plasma forming gas flow rate (slm or kg/s)
m_p	: powder mass flow rate (kg/h)
q_w°	: losses in torch cooling water (W)
r	: radial distance from the torch axis (mm)
R_{th}	: thermal contact resistance ($\text{m}^2\cdot\text{K}/\text{W}$)
T_f	: coating surface temperature ($^\circ\text{C}$)
T_i	: substrate surface temperature after preheating ($^\circ\text{C}$)
T_s	: particle surface temperature (K)
V	: arc voltage (V)
v_g	: plasma gas velocity (m/s)
v_o	: axial gas velocity at the torch nozzle exit (m/s)
v_p	: particle velocity (m/s)
v_r	: cylindrical substrate rotation velocity (rpm)
v_t	: torch translation velocity (m/s)
z_{sp}	: stand off distance (mm)

Greek Symbols

α	: linear expansion coefficient (m/m.K)
δ	: maximum thickness of one bead (μm)
δ_p	: pass thickness (μm)
δ_s	: splat thickness (μm)
Δv	: $v_g - v_p$ (m/s)
η	: thermal efficiency of the torch [$\rho = (V \cdot I - q_w^\circ) / VI$] (%)
κ	: thermal conductivity (W/m.K)
$\bar{\kappa}$: mean integrated thermal conductivity (W/m.K)
κ_p	: particle thermal conductivity (W/m.K)
ν	: Poisson's coefficient (-)
ρ	: specific mass (kg/m^3)
ξ	: flattening degree (-)
	mean integrated thermal conductivity

Abbreviations

A/C	: adhesion/cohesion.
FC	: fused and crushed
PSZ	: partially stabilized zirconia ($\text{ZrO}_2 + 8 \text{ wt}\% \text{ Y}_2\text{O}_3$)
RC	: average cooling rate of a splat ($\text{K}/\mu\text{s}$)

1. INTRODUCTION

Thermal spraying is a widely used technique to provide thick coatings with appropriate functional properties. The process itself is still very complex because more than 60 parameters influence the coating quality⁽¹⁾. The set point determination of the process parameters is often a matter of trial and error and is time consuming. Moreover, the stress build-up in the coating which is determined by the cooling conditions of the droplets on the surface⁽²⁾ and of the successive layers^(3,4), varies with the coating growth owing to the change in the local thermal field. In the actual state of the art for thermal spraying machines, the set point parameters are determined for all the spraying operation duration and do not take into account the changing conditions at the coating's interface. In addition to these changes, industrial thermal spraying practice is submitted to deposit condition fluctuations due to progressive electrodes degradation, random

modifications of heat transfer, changes in thermal limiting conditions, plasma jet fluctuations, powder feed rate variations, powder injection problems and so on. All these facts lead to coatings with limited performances due to the lack of control of defects like cracks, porosity, adhesion/cohesion and lack of reproducibility. These increase manufacturing cost and accordingly limit plasma spraying market share the phenomena involved in the optimization.

To illustrate the complexity of the spraying process, we have chosen partially stabilized zirconia (PSZ with 7 wt% yttria) coatings used as thermal barriers⁽⁵⁾ and we will present successively the phenomena linked to : plasma jets, powder injection, treatment of particles in flight, particles flattening and cooling of resulting splats, coating generation and the correlation between their adhesion/cohesion and the splats formation.

2. PLASMA JETS

The surrounding atmosphere when spraying PSZ is always air and due to zirconia low thermal conductivity, Ar-H₂ mixtures with 20 to 30 H₂ vol% are chosen as plasma forming gases. The effect of H₂ is to increase plasma gas κ ⁽⁶⁾ and enthalpy and thus improve the heat transfer to particles.

For a given torch design, the main parameters which an operator can control are the nozzle internal diameter (i.d.) d , the plasma forming gas flow rate m_g and its composition, the arc current I . The choice of the torch manufacturer can play an important role in the characteristics (temperature and velocity distributions) of plasma jets which can be very different depending on the gas injector and arc chamber design for the same I , m_g and plasma forming gas composition⁽⁷⁾. For a given plasma torch and given working conditions the radial temperature distribution is not very sensitive to d (between 6 and 10 mm) but the length of the hot zone of the plasma jet ($T > 8000$ K) depends on it. For decreasing values of d , the jet velocity v_g increases, and thus the surrounding air pumping increases due to the engulfment process⁽⁸⁾. At the extremity of the plasma jet, the initially cold air bubbles are heated enough to start to mix with the plasma which is cooled more rapidly.

Systematic studies of the jet axial velocity at the nozzle exit v_0 were performed for an Ar-H₂ (25 vol%) mixture. For this torch, a special design of the gas injector⁽⁹⁾ yielded stable conditions, for values of m_g

varying between 37 and 100 slm, with d ranging from 6 to 10 mm (i.e. a section ratio between 1 and 2.8). For example table 1 summarizes the torch working conditions for $I = 600$ A and $m_g = 60$ slm.

d (mm)	6	7	8	10
V (V)	66	64	61	60
η (%)	61	61	59	56

Table 1 : Torch working conditions : $I = 600$ A, 45 slm Ar, 15 slm H_2 .

It is important to notice that V and ρ do not vary very much when d increases from 6 to 10 mm. The jet axial velocity at the nozzle exit was measured with an optical method based on the propagation of the plasma jet luminosity fluctuations⁽¹⁰⁾ and its variations with I , d and m_g were represented by the following empirical relationship.

$$v_0 = 2.42 \cdot 10^{-2} I^{0.44} d^{-1.956} m_g^{0.20} \quad (1)$$

With this coefficient, I is in A, d in m and m_g in kg/s. The above equation shows that, the jet maximum velocity v_0 is almost inversely proportional to the nozzle section area (as it could be expected), varies almost as the square root of the arc current and is not very sensitive to the plasma gas flow rate (when increasing it, more and more gas flows around the plasma column). In the following finally a total flow rate m_g of 60 slm was chosen. Below 60 slm the torches (especially with $d = 9$ or 10 mm), were not very stable for $I > 550$ A and for higher values of m_g the gain in gas velocity was not worth the increased cost of the gas. When increasing too much the arc current, over 600-700 A for a 7 mm i.d. nozzle for example, due to the increased penetration of the surrounding air, the plasma jet length does not change anymore⁽¹¹⁾ while its velocity still increases. The maximum temperature achieved at the nozzle exit is not very sensitive to the arc current value (1000 K between 300 and 600 A) and the main effect when increasing I is to raise the jet diameter at the nozzle exit and reduce the radial temperature gradients. According to our experience, but also to the spraying specifications recommended by the torch manufacturers, typical values of I for $d = 6$ or 7 mm are between 600 and 700 A. For example with 600 A it is possible with our d.c. torch to vary v_0 from 2100 m/s with a 6 mm i.d. nozzle to 770 m/s with the 10 mm

one. It is worth noting that the highest velocity is still subsonic, the sound velocity of the Ar-H₂ (25 vol%) mixture at 14000 K being of the order of 3000 m/s⁽¹²⁾.

In fact the temperature and velocity distributions of the plasma jets are mean values because, due to the arc root restrike mode at the anode, the plasma jets are continuously fluctuating. As suggested by Coudert et al.⁽¹⁰⁾, each time a new arc root is created, a plasma bubble, the column in which the electrical conductivity is high enough, begins to grow. The plasma bubble is then pushed downstream by the plasma flow, partly due to the gas feeding and partly by thermal expansion and M.H.D. forces. When a breakdown occurs the arc is shunted and the bubble partly disconnected from the plasma column giving rise to a flying "puff" travelling with the flow. Thus, in fact, the plasma flow is an heterogeneous medium made of successive puffs of hot gas surrounded by colder layers. According to the measurements of J.F. Coudert and M.P. Planche the frequencies of the restrike mode vary with I, m_g and d (see table 2 for I = 600 A, m_g = 60 slm).

Nozzle i.d. (mm)	6	7	9	10
Restrike mode frequency (kHz)	23.7	18.9	14	10

Table 2 : Evolution with d of the arc root restrike mode frequency.

The residence time of particles within the plasma jet varying for the PSZ powders between 0.4 ms (d_p = 20 μm) and 1.4 ms (d_p = 60 μm), for a 7 mm i.d. nozzle with f = 18.9 kHz a particle "sees" between 10 and 14 successive puffs during its flight and, in spite of its thermal inertia, its impact velocity and surface temperature may be affected by the arc root fluctuations with a succession of hot and cold particles impacting the substrate⁽¹³⁾. This heat transfer problem may also be increased by the particles trajectory fluctuations (see section 3.1).

According to our experiments the nozzle and cathode tip wear may also be not quite negligible. After starting the torch with new electrodes and operating with the same working parameters, the wear of the cathode tip and the beginning of the nozzle erosion reduce the arc voltage. For example with d = 7 mm the voltage drops from 69 V to 64-63 V within 30-45 mn, the arc root restriking frequency decreased from 22 to 19 kHz. Then, the torch parameters do not vary very much during 15-30 h

(depending on the number of times the torch was shut off and restarted). Afterwards suddenly the lifetimes of the anodic spots increases rather fast inducing a high nozzle erosion which modifies erratically the torch working parameters and thus the spraying conditions. This is due to the roughness increase at the anode surface, the arc root residence time increases drastically when the surface becomes too rough.

3. PARTICLES IN FLIGHT

3.1. Particles Injection and Trajectories

The particle trajectories distribution (often called number flux distribution) within the plasma jet was determined by using a 2D laser imaging technique⁽¹⁴⁾. This set-up allows to determine both the laser light scattered by the particles everywhere in the jet and the light emitted by the hot particles ($T > 2500$ K) at the laser wavelength (at distances greater than 40 mm from the nozzle exit). When injecting particles with a carrier gas flow rate (m_{cg}), they have a size distribution, an injection velocity distribution (due to the carrier gas velocity distribution within the injector) and they collide between themselves and with the injector wall resulting in important radial components of their velocity⁽¹⁵⁾. Their trajectories result from the combination of their size and injection velocity distributions and from the relative value of their radial component. When comparing two size distributions : - $45 + 22 \mu\text{m}$ and - $22 + 5 \mu\text{m}$ of fused and crushed (FC) zirconia particles injected inside the 7 mm i.d. nozzle the particles trajectories are the most dispersed⁽¹⁵⁾ for the smaller particles (the carrier gas flow rate has to be high to give the particles a sufficient momentum to penetrate the plasma jet, resulting in a broad injection velocity distribution and the collision rate is high). Moreover, the measurements of the particle jet diameter in the injector direction show that for the (- $45 + 22 \mu\text{m}$) particles, the dispersion effect is almost insensible to m_{cg} up to 6 slm while with the - $22 + 5 \mu\text{m}$ particles the jet is scaled up at each axial position as the carrier gas flow rate is increased⁽¹⁴⁾.

This demonstrates that the collisions between the particles or with the injector wall are more numerous for the small particles. Similar measurements were obtained in the direction orthogonal to the injector however with broader distributions. The maxima of these two number flux distributions define the "mean trajectory"⁽¹⁵⁾ of the particles within the jet.

The optimum mean trajectory, that resulting in the highest velocities and surface temperatures of the particles⁽¹⁵⁾, corresponds to an angle of 3.5° . The values of m_{cg} corresponding to this mean trajectory depend on the plasma gas momentum and particle size distribution. For example Table 3 summarizes the corresponding values for two values of d and an injector i.d. of 1.8 mm. In the following, except when specifically indicated, all tables and figures were obtained with $d = 7$ mm, $I = 600$ A, 45 slm Ar, 15 slm H_2 , internal injection 3 mm upstream of nozzle exit and 1.8 mm in i.d., with FC PSZ particles ($-45 + 22 \mu\text{m}$) and a powder flow rate $m_p = 1$ kg/h.

Particle size	- 22 + 5 μm	- 45 + 22 μm	- 90 + 45 μm
$d = 7$ mm	7.5	5.5	3.5
$d = 10$ mm	4.5	3.5	2

Table 3 : Argon carrier gas flow rate (slm) to achieve an optimum mean trajectory.

It is worth noting that when measuring the signal emitted by the continuum of the plasma jet at the laser wavelength (514.5 nm) this signal is lowered and shifted to the direction opposite to the gas injector when $m_{cg} > 3$ slm. The difficulty of injecting small particles within the plasma jet due to their broad trajectory distribution at the injector exit is illustrated by the radial intensity distribution of the signal scattered by the in-flight particles ($-22 + 5 \mu\text{m}$), measured 5 mm downstream of the nozzle exit (see fig. 1.a).

The injector was vertical in order to inject the particles from bottom to top. It can be clearly observed that the principal maximum of each distribution profile is displaced towards the torch axis center line as m_{cg} is increased from 5 to 8 slm. It is also interesting to note that a minor maximum can be seen at about 7 mm above the torch center line with $m_{cg} = 5$ or 6 slm. This second peak corresponds to particles bypassing the plasma jet and distributed spatially over it. Increasing m_{cg} results in the concentration of the particles inside the plasma jet reducing the bypassing particles. When looking at the distributions of cold and hot particles 45 mm downstream of the nozzle exit (see fig. 1.b) it can be seen that on both sides of the hot particles distribution⁽¹⁶⁾ cold ones are entrained. These cold particles are progressively sucked in the plasma plume, as shown by the measurements, and hit the substrate and coating during spraying where

they may create defects.

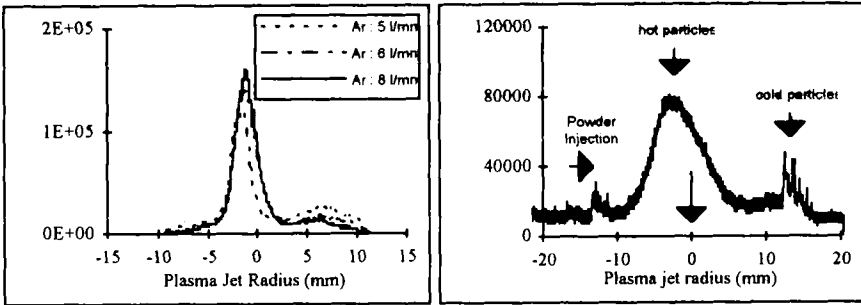


Fig. 1. Particle radial distributions : a) - $22 + 5 \mu\text{m}$ for different m_{CG} , $z_{SP} = 5 \text{ mm}$, b) - $45 + 5 \mu\text{m}$ PSZ $m_{CG} = 4 \text{ slm}$, $z_{SP} = 45 \text{ mm}$.

However the injection problem seems to be complicated by the plasma column arc root fluctuations. The restrike mode induces high voltage ($\pm 30\%$) and thus power fluctuations. According to what has been said about the mean trajectory, depending on the dissipated instant power the mean trajectory of particles is probably fluctuating around that corresponding to the mean power. This is illustrated in fig. 2 which represents two signals emitted by the hot particles acquired randomly each one with an integration period of 13 ms. The signal intensity varies by 30% which corresponds, for a constant temperature, to a flow rate fluctuation of 30%.

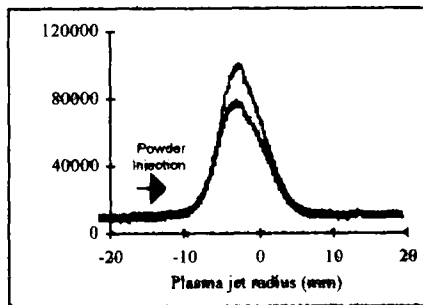


Fig. 2. Fluctuation of hot particles ($- 45 + 5 \mu\text{m}$) radial distribution ($m_{CG} = 4 \text{ slm}$, $z_{SP} = 45 \text{ mm}$).

This dispersion of the particle trajectories was confirmed by the measurements performed with a set-up consisting of two high-speed two-colour pyrometers⁽¹⁷⁾ allowing the determination of the surface temperature, velocity and diameter of a single particle in flight. At the measuring point ($\varnothing = 160 \mu\text{m}$, $l = 160 \mu\text{m}$) disposed on the mean trajectory of the particles at $z_{\text{sp}} = 120 \text{ mm}$ very large velocity (110-250 m/s), diameter (20-50 μm) and surface temperature (2600-4400 K) distributions were obtained⁽¹⁸⁾. Due to the collisions between the particles within the injector and the trajectories fluctuation, the size segregation of the particles in flight is dumped and, at the same location, particles with a size distribution close to the initial distribution can be seen.

3.2. Particle Surface Temperature and Velocity

The statistical measurements of velocity, surface temperature and particle trajectory distributions were performed by LDA, two-color fast (200 ns) pyrometry, and laser fluxmetry⁽¹¹⁾. It is worth noting that the precision of the velocity measurement was $\pm 5\%$ while that of surface temperature measurement was only $\pm 12\%$. In the following all the results will be presented for F.C. particles. When m_p increases there is a load effect⁽¹⁹⁾ and over $m_p = 2 \text{ kg/h}$ the particles slow and cool down. Beside, due to the difficulties in modelling the particle trajectories distribution within the plasma jets, the calculations of the load effect overestimate it. In the following to avoid any load effect all the measurements were performed with $m_p = 1 \text{ kg/h}$.

The influence of the arc current on the particle velocity measured at $z_{\text{sp}} = 100 \text{ mm}$, $r = 4.5 \text{ mm}$ is shown in fig. 3.a for two nozzle diameters. The tendencies predicted by eqn. (1) for the gas flow are good but the exponents in a similar equation giving v_p instead of v_g are not quite the same. This is logical because first the relative velocity Δv plays a role on the particle acceleration and second at $z_{\text{sp}} = 100 \text{ mm}$ v_p is mainly governed by the particles inertia.

It is the same for the gas flowrate, v_p for example depending on $m_g^{0.37}$ instead of $m_g^{0.2}$ for v_g (see fig. 3.b).

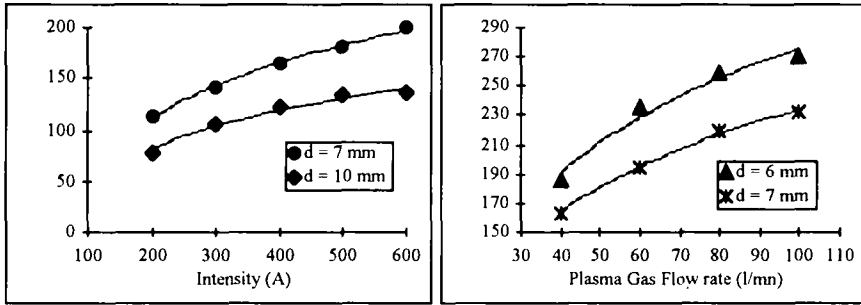


Fig. 3. At $z_{sp} = 100$ mm, $r = 4.5$ mm with $d = 7$ and 10 mm evolution of the particle velocity : a) with the arc current I , b) with the total gas flow rate m_g .

Table 4 summarizes the maximum velocities obtained for different particle size distributions and nozzle i.ds. for $I = 600$ A, 45 slm Ar and 15 slm H_2 .

d_p (μm)	- 90 + 45	- 45 + 22	- 22 + 5
d (mm)			
6	--	220	290
7	130	200	260
10	90	135	170

Table 4 : Maximum velocities (m/s) achieved by particles of different diameters with different nozzle i.ds..

It is worth noting that with $d = 7$ mm T_s drops to a maximum value of 3200 K with - 90 + 45 particles instead of 4000 K with - 45 + 22 μm . In the same conditions the smallest distribution gives $T_s = 4100$ K. However with them in the hot core of the plasma the evaporation is tremendous as shown when measuring the intensity of ZrI lines, those values are two order of magnitude higher than with the - 45 + 22 μm particles. The corresponding radial distribution measured at $z_{sp} = 100$ mm shows that the maximum particle velocity is obtained close to the jet axis (at a location corresponding to the optimum trajectory) and it decreases in a ratio of about 2 in the fringes of the spray cone. For T_s , the maximum seems to be (according to the precision of the measurements) at the jet axis and the radial drop is much less than that of velocity. In the fringes of the spray

cone the particles have longer residence times in colder area of the plasma jet. For v_p and T_s the load effect is present. However in the spray cone fringes where the particle number flux is almost two order of magnitude lower, the load effect is much less sensitive for T_s . The surface and center temperature of zirconia particles (90, 60, 30 μm) along their mean trajectories were calculated using the measured temperature and velocity distributions of the plasma flow⁽¹⁵⁾.

These calculations show that if the 60 μm particles are at the limit of a complete molten state, those with a smaller diameter are completely molten.

An important heat propagation phenomenon being encountered with FC zirconia particles in an Ar-H₂ plasma⁽²⁰⁾, as agglomerated or agglomerated and sintered particles exhibit lower κ_p than FC ones, the heat propagation phenomenon is enhanced⁽²¹⁾ with them, resulting in particles which are not fully molten upon impact. Thus all the experiments presented in the following were made with FC particles.

4. COATINGS GENERATION

4.1. Substrate and Coating Temperature Monitoring during Spraying

Monitoring substrate and coating temperature during spraying is really a key point to control coating adhesion/cohesion (A/C) and residual stresses distribution^(4,22-24).

Spraying was achieved by using the set-up already described^(22,24) and consisting of a cylindrical substrate holder (substrate \varnothing 25 mm, δ = 5 mm) 110 mm in external diameter rotating at a constant velocity v_r in front of a plasma torch translated back and forth at a constant velocity v_t parallel to the cylinder axis (with the torch axis orthogonal to that of the cylindrical holder). The surface temperature of substrates during their preheating and coatings during spraying was followed by an IR monochromatic pyrometer (5.2 μm , 10 Hz). The heating was achieved by the plasma jets. According to previous heat flux and particles in flight measurements, a stand off distance z_{sp} = 100 mm was chosen. Beside the heating by the plasma jet plume, the heat flux brought by the particles is not negligible at all, especially for thick passes (their thickness δ_p depends on v_r , v_t and m_p)⁽²⁵⁾. The thicker are the passes the higher is the temperature within them (κ_p

(PSZ) $\sim 1\text{-}2 \text{ W/m.K}$). The cooling of substrate and coating was achieved by air jets blown through machined slots ($1 \times 28 \text{ mm}^2$) either one disposed 5 mm in front of the cylindrical holder in the direction opposite to the plasma jet (R) or one blown orthogonally to the plasma jet 20 mm before the substrate holder and 12 mm below the jet axis (B). B reduces in a ratio up to 6 the heat flux from the plasma plume. However the effect of B is also to reduce the velocity of the impacting particles by 10 to 15% and their surface temperature by 15%. The use of B or R or B+R induces surface temperature fluctuations ΔT_s due to substrate holder rotation and torch translation. ΔT_s depends also, for given spraying parameters, on δ_p . For example table 5 summarizes the preheating temperatures T_i of stainless steel substrates measured respectively opposite to the plasma jet (at an angle of 180° from the jet axis), over the plasma jet plume (at an angle of $+20^\circ$ from the torch axis) and below the plasma jet plume (at an angle of -20° angle from the torch axis) and the coating surface temperatures T_f measured in the same conditions with pass thicknesses of $20 \mu\text{m}$ and a bead overlapping of 50%(25). Preheating with the plasma jet allowed to achieve preheating temperatures between 250 and 500°C in less than 90 s, thus reducing substrate oxidation during this preheating phase.

Cooling conditions	B + R	R (30 scmh)	R (5 scmh)
T_i preheating temperature	170 ± 20	380 ± 15	500 ± 20
T_f coating temperature	250 ± 30	550 ± 50	650 ± 30

Table 5 : Preheating T_i and coating T_f temperatures measured opposite to the plasma jet and their fluctuations ΔT ($m_{cg} = 4,5 \text{ slm}$, $\delta_p = 20 \mu\text{m}$).

It can be readily seen that ΔT_s is not negligible at all, the low response time of the pyrometer (10 Hz) probably underestimating it.

Beside the coating formation, single particle flattenings and resulting splat coolings were studied with two fast (100 ns) two color pyrometers (17,18,26,27), the substrates being protected from plasma heat flux by a water cooled screen opened during about 1 s. The substrates were preheated by a resistor which, according to the heating time (about 500 s), induces more oxidation than when preheating is achieved in less than 90 s with the plasma jet. It was the same for the collection of the splats all over the spray cone by a method derived from the line-scan test(22).

4.2. Substrate Roughness

The substrates for the coatings were made of stainless steel 304 L ($\alpha = 18 \times 10^{-6}$ m/m.K, $E = 203$ GPa). They were sand blasted with a pressure type machine⁽²⁸⁾ to obtain a R_a of 9 ± 2 μm .

To study the splat formation the substrates summarized in table 6 were used.

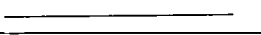
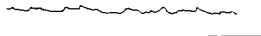
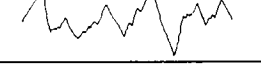
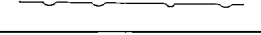
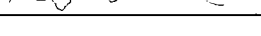
Substrate nature	R_a (μm)	Roughness profile
304 L : mirror polished	0.05	
304 L : electropolished	0.4 ± 0.1	
304 L : grit blasted	9 ± 2	
Ground plasma sprayed PSZ	0.2 ± 0.05	
As sprayed PSZ	4 ± 1	

Table 6 : Substrates used to study splat formation : surface treatment, R_a and roughness profiles.

The PSZ substrates, 350-400 μm thick were sprayed after their steel substrates were preheated to 380°C. They were either ground (in this case the roughness corresponds mainly to pores or holes between adjoining splats) or as sprayed (in this case compared to the initial 304L roughness, the peaks and undercuts are smoothed).

4.3. Splat Formation

4.3.1. Individual Splats

Two high speed (100 ns) two-color pyrometers were used^(17,18,26,27) to determine for a single particle its diameter prior to impact, its flattening degree ξ , flattening time and the resulting splat average cooling rate RC . When possible i.e. on as mirror-polished substrates the values of ξ were also calculated from the splat thicknesses. The measurements were performed at $z_{sp} = 100$ mm at the location of the optimum trajectory but it has to be kept in mind that at that point the

velocity, surface temperature and diameter distributions of the impacting particles were very broad (see section 3.1).

In order to determine the thermal contact resistance R_{th} between the splat and the substrate a 1D model of the splat cooling was developed by A. Vardelle et al.(18,26). It is based on the assumption that the cooling of a splat is mainly governed by the quality of contacts with the substrate. This model was used to predict the temperature fields within the splat and the substrate, the position and velocity of the solidification front and its RC, defined as the time necessary for the splat surface to reach a given temperature (for example 2000 or 1000 K). The comparison of the experimental values of RC with those calculated for different values of R_{th} allowed to determine for a splat, which thickness was measured, the value of R_{th} . Such calculations performed for 304 L and zirconia substrates show (see fig. 4.a and b) the drastic influence on RC of δ_s and R_{th} when $R_{th} < 10^{-7} \text{ m}^2\cdot\text{K}/\text{W}$. However such a comparison is not possible for extensively fingered splats the model being established for a cooling disk.

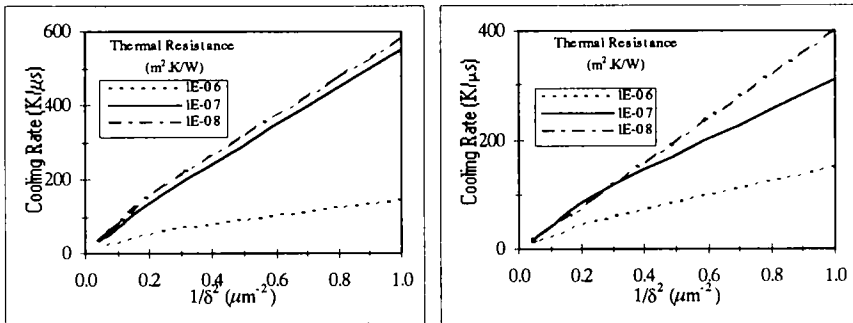
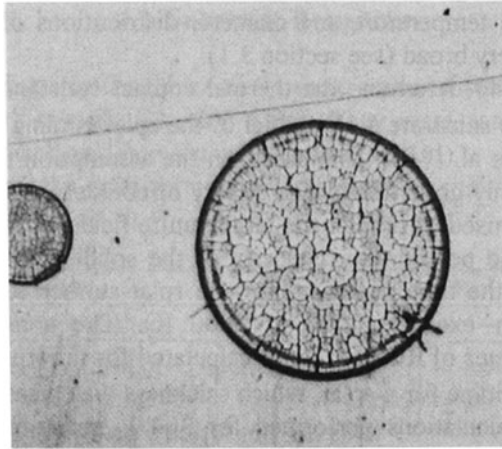


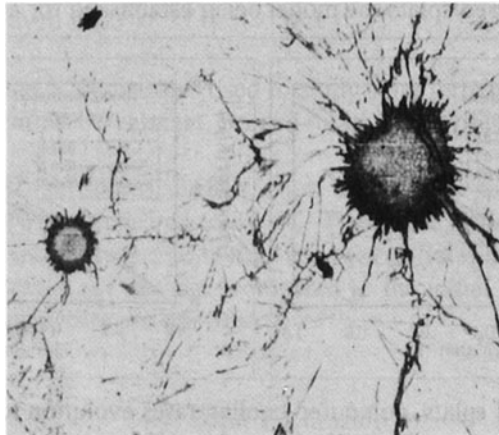
Fig. 4. For PSZ splats, computed cooling rates evolution with the inverse of the square of splat thickness for different values of R_{th} :
 a) on 304 L, b) on PSZ substrate(27).

a) Smooth substrates

On 304 L mirror-polished ($R_a \sim 0.05 \mu\text{m}$), the splats sprayed with the d.c. torch $d = 7 \text{ mm}$ (mean impact velocity of 200 m/s, see table 4), exhibit almost perfect disk shapes with a microcrack network, corresponding to the quenching stresses relaxation(2,3), covering the whole splat surface (see fig. 5.a) provided the substrate is not oxidized and its temperature is over 200°C (18,26,27,29).



a)

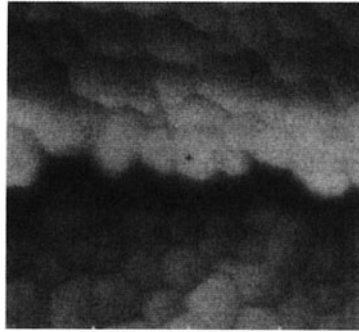


b)

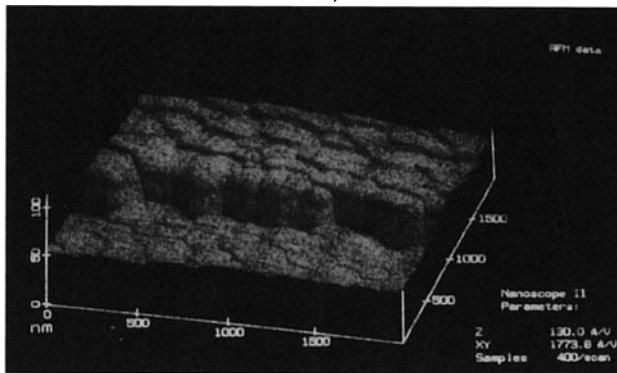
Fig. 5. PSZ splats collected on 304 L substrates ($R_a \sim 0.05 \mu\text{m}$) :
a) hot substrates (300°C), b) cold substrates (75°C).

The microstructure of the splats was examined by Atomic Force Microscopy (AFM). Fig. 6.a and b give a typical example of a small region ($2000 \times 2000 \text{ nm}^2$) of the splat including a microcrack. The columnar structure covers the whole splat (except may be its rim see fig. 5.a) with columns which mean diameter is of the order of 150 nm . At the edge of the

splat as the contact with the substrate is not excellent due to its curling, as already shown for alumina⁽³⁰⁾, the columnar structure grows parallel to the substrate. With a mean impact velocity of 200 m/s, the splat thicknesses are between 0.65 and 1.05 μm .



a)



b)

Fig. 6. Atomic Force Microscopy of a small area ($2 \times 2 \mu\text{m}^2$) of a splat such as that represented in fig. 5.a : a) Top view, b) Side view.

RC values of $643 \text{ K}/\mu\text{s}$ (see table 7 col. 3) reflect the intimate contact between the splats and the substrate. The comparison between the experimental and calculated RC yields in $R_{\text{th}} \sim 10^{-7} - 10^{-8} \text{ m}^2 \cdot \text{K}/\text{W}$ (i.e. almost a perfect contact, see fig. 4.a).

Below 150°C the splat is extensively fingered (see fig. 5.b) and its mean diameter is 20 to 40% lower than that obtained on the hot substrate. As soon as oxidation has proceeded, even at high temperature, the splats

are also extensively fingered. This can be observed either when letting the substrate preheated for more than 150 s at 500°C before spraying or, after a such heating, letting it cool down to room temperature and heating it again at 200°C in less than 90 s before spraying. Such an experiment demonstrates that the effect of preheating is not to improve the particle wettability by eliminating the water staying at the surface but that the splats loose their disk shape as soon as the oxide layer thickness is over about 50 nm.

When considering the spray cone as a whole with 3000-5000 collected splats the same effect is observed : disk shape splats (mean shape factor $SF \sim 0.91 \pm 0.2$) with a mean diameter D of $103 \pm 34 \mu\text{m}$ corresponding to $\delta_s = 0.85 \mu\text{m}$ on hot non oxidized substrates against extensively fingered splats on cold substrates ($D = 62 \pm 19 \mu\text{m}$ and $SF = 0.67 \pm 0.2$). The lower value of D on the cold substrates is due to the liquid particle splashing at the end of the impact when the viscous energy is dissipated.

As soon as B is used to monitor T_f the resulting splats exhibit a more jagged aspect and their thickness increases drastically (see table 7, exp. 4). This is probably due to the cooling and slowing down of the particles prior to their impact, the colder layer surrounding the hot core of the impacting particle reducing its flattening. However, even if precise measurements with the pyrometer were not performed, the contact between the splat and the substrate seems to be very good according to the microcrack network covering its whole surface. With a more important thickness RC must be lower than without B , according to the cooling model (see fig. 4.a).

Of course when reducing the particle velocity (by using a 10 mm i.d. d.c. torch or a rf torch (see exp. 1 and 2 of table 7) δ_s increases too and the corresponding RC should decrease (assuming $R_{th} \sim 10^{-7} \text{ m}^2\text{K/W}$ according to the disk shaped splats and their microcrack network). When looking at the shape factors, it can be seen that they are the best for the RF plasma torch (see table 7 exp. 1 and fig. 7.a) : the particles are very well molten according to their much longer (one order of magnitude) residence time. However as soon as $T_i < 150^\circ\text{C}$ the splats exhibit more distorted shapes (compare fig. 7.b and 5.b). than when using the d.c. torch with $d = 7 \text{ mm}$ (the SF could not be measured as most of the splats were detached during the substrate handling)⁽²⁹⁾.

Experiment number	1	2	3
Substrate nature	304 L	304 L	304 L
Substrate roughness Ra (μm)	0.05	0.05	0.05
Particle velocity (m/s)	20	135	200
Flattening degree	3.6	4.6	5
Shape factor	0.98 ± 0.04	0.88 ± 0.2	0.91 ± 0.2
Splat thickness (μm)	2.4	1.1	0.85
Cooling rate (K/μs)	--	--	643
R _{th} (m ² .K/W)	--	--	10 ⁻⁸ - 10 ⁻⁷
Experiment number	4	5	6
Substrate nature	304 L*	304 L**	PSZ
Substrate roughness Ra (μm)	0.05	0.4	0.2
Particle velocity (m/s)	200	200	200
Flattening degree	--	4.8	4.7
Shape factor	0.85 ± 0.2	0.82 ± 0.2	0.85 ± 0.2
Splat thickness (μm)	1.6		
Cooling rate (K/μs)	--	123	113
R _{th} (m ² .K/W)	--	10 ⁻⁶	10 ⁻⁸ - 10 ⁻⁷

Table 7 : Particle parameters at impact : for hot substrates at 250-300°C(27,29).

* splats obtained with an air barrier B between substrate and plasma plume.

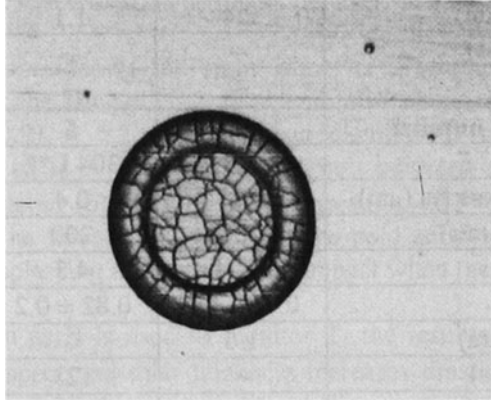
** electropolished substrates.

When using an electropolished substrate the splats exhibit also a more jagged aspect, their thickness being however about the same as that of those collected on the polished surface (Ra ~ 0.05 μm). Surprisingly RC is only of the order of 100 K/μs (see table 7 exp. 5) which is probably due to the oxidation of this surface more sensitive than that of the as mirror polished one.

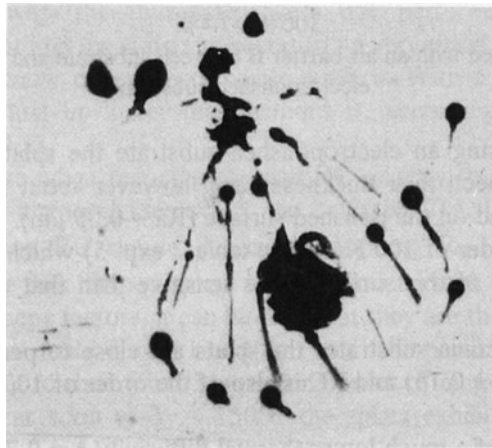
With zirconia substrates the splats are close to perfectly lenticular ones (SF ~ 0.98 ± 0.15) and RC is also of the order of 100 K/μs (see table 7, exp. 6).

In spite of a much lower thermal diffusivity $a = 0.7 \cdot 10^{-6} \text{ m}^2 \cdot \text{s}^{-1}$ for PSZ against $5.2 \cdot 10^{-6} \text{ m}^2 \cdot \text{s}^{-1}$ for 304 L, the values of RC for PSZ and electropolished substrates are about the same. The comparison of the experimental and calculated RC values yields in excellent values of R_{th} ~ 10⁻⁷ - 10⁻⁸ m².K/W for PSZ substrates (a molten material wets well its

own solid, which is not however the case below 200°C for the splats) while for 304 L electropolished and oxidized by the preheating $R_{th} \sim 10^{-6} \text{ m}^2 \cdot \text{K/W}$ (see table 7 exp. 5). It is worth noting that according to the slower cooling down time to a splat temperature of 1000 K (20 μs against 3 μs on a steel substrate) AFM shows that the size of the columns increases, probably due to their coalescence.



a)



b)

Fig. 7. Splats collected on 304 L substrates ($R_a \sim 0.05 \mu\text{m}$), RF plasma spraying⁽²⁹⁾ : a) hot substrate (300°C), b) cold substrate (75°C).

b) Rough substrates

As surface roughness increases, the splashing of the molten droplets upon impact increases resulting in star shaped splats on hot (300°C) substrates.

Of course as soon as the temperature is below 75°C the particle is almost completely exploded. Table 8 summarizes the results obtained on 304 L and PSZ substrates.

Substrate nature	304 L	PSZ
Substrate roughness Ra (µm)	9 ± 2	4 ± 1
Flattening degree	4.2	4.3
Cooling rate (K/µs)	133	86

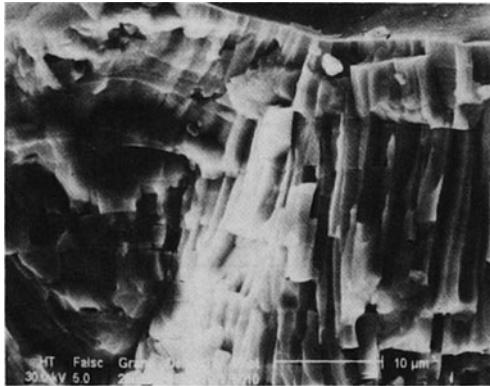
Table 8 : Splat parameters for hot 300°C rough 304 L and PSZ substrates (see table 6).

On both substrates, the mean flattening degree is about the same of the order of 4.2. It should be noted that the pyrometric technique used in this study collected the whole light emitted by the hot material, including splash products. Thus this method tends to overestimate the size of the splats. The standard deviation is greater than that determined on smooth substrates because of the scattering of the impinging droplets by surface asperities. The cooling rates are similar to those obtained on smoother PSZ (Ra = 0.2 µm) and steel (Ra = 0.4 µm) substrates. As emphasized by previous results⁽³¹⁾ the thickness of the splats on rough substrates being increased, such high cooling rates could be explained by a "better" local contact, which has to be checked.

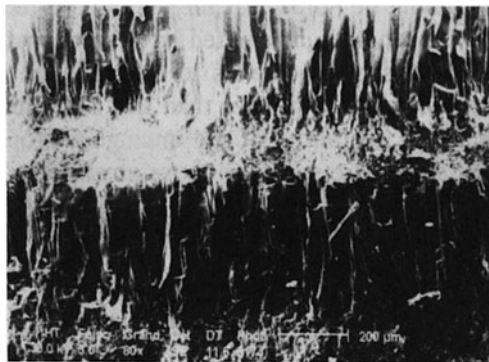
4.4. Beads and Coatings Formation

The beads formation was systematically studied at the laboratory by Haddadi et al.⁽³²⁾ by varying the torch velocity between 1.04 m/s and 10 mm/s corresponding respectively to $\delta = 3 \mu\text{m}$ (about 3 layered splats) and $\delta = 500 \mu\text{m}$ (about 500 layered splats). Provided $T_f > 300^\circ\text{C}$, whatever may be their thicknesses, the SEM fracture micrograph of the beads shows a columnar growth structure (see fig. 8.a) from the bottom to the top of the bead⁽³²⁾.

However after spraying one bead, when coming back with the torch to spray the 100% overlapping second bead, the interface between both is unfortunately not as regular as the columnar growth within each bead.



a)



b)

Fig. 8. SEM fracture micrograph of : a) the top part of a 500 μm thick bead, b) two overlapped 500 μm beads.

Passes with beads overlapping at 50% were realized with the set-up described in section 4.1. Two types of coatings were sprayed. One with passes about 5 μm thick and one with passes 30 μm thick. In both cases the XRD has shown 100% t'phase. When spraying with coating and substrate kept below 150°C the columnar growth is quite erratic, especially close to the substrate (probably in good connection with the extensively fingered

splats). When spraying with preheating to 300°C the columnar growth all through the pass was observed with also a disturbed region at the interface between two successive passes.

4.5. Coatings Adhesion/Cohesion

PSZ (- 45 + 22 μm) deposits were built up with the 7 mm i.d. nozzle d.c. plasma torch on stainless steel (304 L) substrates varying the preheating time from 0 to 900 s in order to obtain, at the interface, various thicknesses of oxide layers. Time 0 corresponds to no preheating at all. Table 9 presents the adhesion/cohesion results obtained for preheating temperatures of 300°C and 500°C.

Preheating (°C)	Preheating time (s)	Adhesion (MPa)
No	0	20 ± 2 (A)
300	30	33 ± 3 (A)
300	60	50 ± 2 (C)
300	300	40 ± 2 (A)
300	900	31 ± 4 (A)
No	0	19.5 ± 2 (A)
50	120	64 ± 5 (C)
500	300	49 ± 2 (A)
500	900	45 ± 2 (A)

Table 9 : Zirconia coating adhesion/cohesion as a function of the preheating time (A : purely adhesive failure, C : purely cohesive failure).

When increasing the preheating time, the coating adhesion first increased and reached a maximum value, for about 1 or 2 minutes preheating time depending on preheating temperature, and then decreased when the preheating time became too long. This improvement of adhesion for short oxidation times, leading to thin oxide layers (below 30 nm), can be attributed to the well adherent splats on the substrate when T_s is over 150°C.

When the oxidation time was longer than 2 minutes, a decrease of the adhesion was noticeable. In these cases the fracture seemed to take place inside the oxide layer at the interface coating-metal which might be less adhesive or cohesive than the deposited zirconia layer.

Some assumptions could be given to explain why adhesion is higher when the substrates were preheated to 500°C compared to 300°C. The first one is that the kinetic growth of the oxide layer is different for these two temperatures, leading at 500°C to a more cohesive and adhesive layer. A second reason may be the thermal cycling of the deposits during deposition due to the torch heat flux on one side and the cooling air jet on the other side. So, as almost no air cooling was applied when spraying at 500°C (see table 5), the thermal cycling was less important in this case than when spraying at 300°C where a high cooling rate was necessary to maintain this temperature (see table 5).

When spraying with a d.c. torch $d = 10$ mm (lower particle impact velocity see table 7, exp. 2), the same results were obtained except that at the maximum the A/C values were at the best of the order of 30 MPa at preheating temperature of 300°C.

CONCLUSION

The adhesion/cohesion (A/C) of partially stabilized zirconia (PSZ) coatings depends on the splat morphologies, the contact between them and between successive beads and passes. This study has shown that the contacts between the splats and that between splats and substrate all over the spray cone are closely linked to the substrate or previously deposited layers temperature during spraying. Below about 150°C the splats, either on rough or smooth surfaces, are extensively fingered with up to 50% of the impacting droplets splashed away and they present a poor contact with the underlying surface. Over 200°C the splats exhibit an excellent contact with their substrate with cooling rates of the order of 100 K/ μ s (whatever may be the substrate nature 304 L steel provided it is not oxidized i.e. with an oxide layer thickness below 30 nm or PSZ). When the temperature during spraying is maintained over 300°C the columnar growth observed within single splats can be also seen through the layered splats, from the bottom to the top of the resulting bead (up to 500 layered splats) and the same phenomena is observed within one pass provided the cooling of the bead surface is only a few tens of Kelvin between two successive overlapping beads. The surface temperature monitoring of the beads and passes is probably one of the key point to achieve coatings with very high A/C values and the use of different air cooling systems seems also to play a role in the splats formation.

The A/C of the coatings increases with the preheating temperature (provided the substrate oxidation is limited) inducing the coalescence of the columns, however a compromise has to be found with the residual stresses, especially that due to expansion mismatch which also increases with the preheating temperature. The A/C of the coatings also increases with the impact velocity of the particles (provided they are fully molten upon impact) which control the splat thickness δ_s (from $\sim 1 \mu\text{m}$ at 200 m/s to $\sim 3 \mu\text{m}$ at 20 m/s) and thus their cooling rate (roughly proportional to $1/\delta_s^2$). The particle velocity for a given size distribution (in our study - 45 + 22 μm PSZ fused and crushed particles) and a given plasma gas composition (Ar 75 vol% and H₂ 25 vol%) depends on that of the plasma jet itself linked to the square root of the arc current and the inverse of the d.c. torch nozzle diameter d (the effect of the plasma gas flow rate being rather weak). For the studied torches ($6 \leq d \leq 10 \text{ mm}$), $d = 7 \text{ mm}$ seems to be a good compromise to achieve A/C values over 60 MPa : below that the jet diameter is reduced and more particles do not penetrate within the jet. The injection problem is really one of the key point to achieve well molten particles upon impact, due to the particle size and injection velocity distributions and also to the particle collision mainly with the injector wall, the trajectories are very dispersed at the injector exit. Thus the particles impacting at a given point of the substrate have a size distribution almost similar to that of the initial particle distribution. Beside the particles by passing the plasma jet when injecting them and sucked in the plasma plume, the arc root fluctuations at the anode induce high power fluctuations ($\pm 30\%$) and result in particle mean trajectory fluctuations. These injection problems with many unmolten small particles impacting on the substrate and already deposited layers are probably also among the key points to improve the coatings A/C values especially for the unmolten particles trapped between two successive beads an passes.

REFERENCES

1. Fauchais P. and M. Vardelle, *Pure and Appl. Chem.* **66** (6) (1994) 1247-1258.
2. Kuroda S. and T.W. Clyne, *Thin Solid Films* **200** (1991) 49-66.
3. Kuroda S. Fukushima and S. Kitahara, *Vacuum* **41** (4-6) (1990) 1297-1299.
4. Gill S.C. and T.W. Clyne, *Metall. Trans. B.* **21** (1990) 377-385.

5. Gruninger M.F. and M.V. Boris, in *Thermal Spray : international advances in coatings technology*, (Pub.) ASM Int. Oh, USA (1992) 975-982.
6. Pateyron B., M.F. Elchinger, G. Delluc and P. Fauchais, *Plasma Chemistry, Plasma Processing*, **12** (4) (1992) 421-448.
7. Roumilhac Ph., J.F. Coudert and P. Fauchais, *Mat. Res. Soc. Symp. Proc.* **190** (1991) 227-238, (Pub.) MRS.
8. Pfender E., J. Fincke and R. Spores, *Plasma Chemistry, Plasma Processing*, **11** (4) (1991) 529-544.
9. Boncoeur M., P. Fauchais, A. Grimaud and G. Schnedecker, *Torche à plasma d'arc à stabilisation par gainage gazeux*, French Patent 94.11949, Oct. (1984).
10. Coudert J.F., M.P. Planche and P. Fauchais, *Plasma Chemistry, Plasma Processing* **15** (1) (1995) 47-70.
11. Fauchais P., J.F. Coudert, M. Vardelle, A. Vardelle and A. Denoirjean, *Journal of Thermal Spray Technology* **1** (2) (1992) 117-128.
12. Pateyron B., M.F. Elchinger, G. Delluc and P. Fauchais, *Soud velocity in different reacting thermal plasma systems*, accepted in *Plasma Chemistry, Plasma Processing*.
13. Fincke J.R. and W.D. Swank, in *Thermal Spray Coatings : Properties, Processes and Applications*, (Pub.) ASM Int. Oh (1992) 193-198.
14. Li K.I., M. Vardelle, A. Denoirjean and P. Fauchais, *Monitoring the particle injection and trajectory distribution during plasma spray process*, in the proc. of 3rd Thermal Plasma Processing Symposium, Aachen, Sept. (1994) to be published by V.D.I. Düsseldorf, G.
15. Vardelle M., A. Vardelle and P. Fauchais, *J. of Thermal Spray Technology* **2** (1) (1993) 79-91.
16. Li K.I., M. Vardelle and P. Fauchais, *Comparison between single and double flow powder injectors in plasma spraying process*, to be published in proc. of NTSC95, (Pub.) ASM Int. Oh USA.
17. Vardelle M., A. Vardelle, P. Fauchais and C. Moreau, *Meas. Sci. Technol.* **5** (1994) 205-212.
18. Vardelle A., M. Vardelle, P. Fauchais and D. Gobin, *NATO ASI Series (ed.) T.W. Davis, Series E : Applied Sciences* **282** (1995) 95-121.
19. Vardelle A., M. Vardelle, P. Fauchais, P. Proulx and M.I. Boulos, in *Thermal Spray : Int. Advances in Coatings Technology*, Pub. ASM Int., Oh, USA (1992) 755-766.

20. Bourdin E., P. Fauchais and M.I. Boulos, *Int. J. Heat Mass Transfer* **26** (1983) 567-582.
21. Vardelle M., A. Vardelle, A. Denoirjean and P. Fauchais, *Mater. Res. Soc. Symp. Proc. MRS* **190** (1991) 175-183.
22. Bianchi L., A. Grimaud, F. Blein, P. Lucchese and P. Fauchais, *J. of Thermal Spray Technology* **4** (1) (1995) 59-66.
23. Kuroda S., T. Dendo, S. Kitahara, *J. of Thermal Spray Technology* **4** (1) (1995) 75-84.
24. Mellali M., P. Fauchais, A. Grimaud, Influence of substrate roughness and temperature on alumina coatings adhesion-cohesion, accepted in *J. of Surface Coating Technology*.
25. Monerie-Moulin F., F. Gitzhofer, P. Fauchais, M.I. Boulos and A. Vardelle, *J. of High Temp. Chem. Processes*, (3) **1** (1992) 249-258.
26. Vardelle M., A. Vardelle, A.C. Leger, P. Fauchais and D. Gobin, *Journal of Thermal Spray Technology* **4** (1) (1995) 50-58.
27. Leger A.C., M. Vardelle, A. Vardelle, B. Dussoubs and P. Fauchais, Splat formation : ceramic particles on ceramic substrates, to be published in *Proc. of NTSC95 (Pub.) ASM Int. Oh USA*.
28. Mellali M., A. Grimaud and P. Fauchais, Parameters controlling the sand blasting of substrate for plasma spraying, *Thermal Spray : International Advances in Coatings Technology (Pub.) ASM Int. Oh, USA* (1994) 227-232.
29. Bianchi L., A. Denoirjean, P. Lucchese and P. Fauchais, Zirconia splat formation and resulting coating properties, to be published in *Proc. of NTSC 95 (Pub.) ASM Int. Oh USA*.
30. Bianchi L., P. Lucchese, A. Denoirjean and P. Fauchais, Microstructural investigation of plasma sprayed alumina splats, to be published in *Proc. of NTSC 95 (Pub.) ASM Int. Oh USA*.
31. Moreau C., P. Gongeon and M. Lamontagne, *Journal of Thermal Spray Technology* **4** (1) (1995) 25-33.
32. Haddadi A., F. Nardou, A. Grimaud and P. Fauchais, Generation of the first layers of zirconia plasma sprayed coatings, correlation between splat layering and spraying parameters, to be published in *Proc. of NTSC 95 (Pub.) ASM Int. Oh USA*.